Informing Deep Argo array design using Argo and full-depth hydrographic section data[*]

GREGORY C. JOHNSON[1], JOHN M. LYMAN[1,2], AND SARAH G. PURKEY[3]

[1]*NOAA/Pacific Marine Environmental Laboratory, Seattle, Washington*

[2]*Joint Institute for Marine and Atmospheric Research, University of Hawaii at Manoa, Honolulu, Hawaii*

[3]*Lamont-Doherty Earth Observatory, Columbia University, Palisades, New York*

for *Journal of Atmospheric and Oceanic Technology*

submitted 7 July 2015

revised 19 August 2015

accepted 23 August 2015

doi:10.1175/JTECH-D-15-0139.1

[*] Pacific Marine Environmental Laboratory Contribution Number 4351, JIMAR Contribution Number 15-391.

Corresponding author address: Gregory C. Johnson, NOAA/Pacific Marine Environmental Laboratory, 7600 Sand Point Way NE Bldg. 3, Seattle, WA 98115.

E-mail: gregory.c.johnson@noaa.gov

ABSTRACT:

Data from full-depth closely sampled hydrographic sections and Argo floats are analyzed to inform the design of a future Deep Argo array. Here standard errors of local decadal temperature trends and global decadal trends of ocean heat content and thermosteric sea level anomalies integrated from 2000–6000 dbar are estimated for a hypothetical 5º lat. x 5º long. x 15-day cycle Deep Argo array. These estimates are made using temperature variances from closely spaced, full-depth CTD profiles taken during hydrographic sections. The temperature data along each section are high-passed laterally at a 500-km scale, and the resulting variances averaged in 5º x 5º bins to assess temperature noise levels as a function of pressure and geographic location. A mean global de-correlation time scale of 62 days is estimated using temperature time series at 1800 dbar from Argo floats. The hypothetical Deep Argo array would be capable of resolving, at one standard error, local trends from < 1 mºC decade^{-1} in the quiescent abyssal North Pacific to about 26 mºC decade^{-1} below 2000 dbar along 50ºS in the energetic Southern Ocean. Larger decadal temperature trends have been reported previously in these regions using repeat hydrographic section data, but those very sparse data required substantial spatial averaging to obtain statistically significant results. Furthermore, the array would provide decadal global ocean heat content trend estimates from 2000–6000 dbar with a standard error of ±3 TW, compared to a trend standard error of ±17 TW from a previous analysis of repeat hydrographic data.

1. Introduction

The international Argo Program (Roemmich et al. 2009) reports over 100,000 upper-ocean profiles of temperature and salinity per year. The Argo array first achieved its target of 3,000 freely drifting autonomous CTD-equipped floats in November 2007. Argo floats drift with the currents at a nominal pressure of 1000 dbar, leaving that isobar nominally every 10 days to profile between a target pressure of 2000 dbar and the surface, sampling as they ascend. The floats are nominally spaced at 3º x 3º intervals, and the array provides seasonally unbiased sampling around the globe for the upper half of the ocean volume, except in shallow (generally < 1000–2000 dbar) or ice covered waters. Argo is gradually expanding into seasonally ice-covered regions (Klatt et al. 2007), and ice-tethered profilers (Toole et al. 2011) have sampled regions of the Arctic between about 750 and 10 dbar since 2004.

However, the deeper half of the ocean volume below the 2000-dbar sampling limit of conventional Argo floats is currently much more sparsely sampled. As of 7 July 2015, the World Ocean Database (http://www.nodc.noaa.gov/OC5/SELECT/dbsearch/dbsearch.html) contained 39,352 high-resolution CTD profiles with data extending to at least 3000 m for all time. For the year 2008 there were only 515 high-resolution CTD profiles with data extending to at least 3000 m in the database, mostly concentrated along a few densely sampled quasi-synoptic hydrographic sections, compared with 113,512 spatially and temporally well distributed CTD profiles of the upper ocean from floats.

Regardless of data limitations, the abyssal ocean (here > 4000-m depth) exhibited a detectible, albeit with large uncertainty, warming trend from 1992–2005 of about 5 mºC

59 decade^{-1} in the global mean with deep (> 2000 m) trends closer to 30 mºC decade^{-1} in the
60 Southern Ocean (Purkey and Johnson 2010). The largest deep long-term warming trends
61 we have found published are 130 mºC decade^{-1} from 1980–2010 estimated from repeated
62 measurements in the deep Greenland Sea (Somavilla et al. 2013). This latter trend is
63 similar in magnitude to the global average trend in sea-surface temperature warming from
64 1970–2014 (~115 mºC decade^{-1}) using the NOAA ERSST Analysis (Smith et al. 2008).
65 Deep variability in temperature and salinity can reflect variations in deep convection that
66 connects the substantial heat capacity of the deep ocean directly to the ocean surface and
67 also reflect changes in circulation. For instance, the deep Greenland Sea warming is a
68 direct result of the cessation of deep wintertime convection in that region, with a resultant
69 reversal in deep flow between the Greenland Sea and the Arctic Ocean (Somavilla et al.
70 2013). Variations in deep convection in locations such as the Labrador Sea (Yashayaev
71 2007) are likely to at least contribute in part to deep North Atlantic heat content
72 variations (Mauritzen et al. 2012). The waters of southern origin that fill the majority of
73 the deep and abyssal ocean (Johnson 2008) mostly cascade down in dense plumes from
74 the Antarctic continental shelf (Orsi et al. 1999). However, open ocean convection in
75 features such as the Weddell Polynya of the mid-1970s have also played a role (Gordon
76 1982) in ventilating the abyss in the Southern Ocean. The resulting Antarctic Bottom
77 Waters (Orsi et al. 1999) spread north (Lumpkin and Speer 2007) and, as noted above,
78 have been warming in recent decades (Purkey and Johnson 2010).
79 Ocean heat content increases account for over 90% of the warming in the Earth's
80 climate from 1971–2010 (Rhein et al. 2013). Globally, ocean heat content from 2000–
81 6000 m has been estimated to increase during 1992–2005 from an analysis of repeat

hydrographic data by the equivalent of 0.07 ±0.03 W m^{-2} (uncertainty recalculated as one standard error of the mean) applied over the surface area of the Earth (Purkey and Johnson 2010), similar to the rate of heat gain (equivalent to 0.06 ±0.006 W m^{-2}) estimated deeper than 3000 m from 1985–2006 using data assimilation output (Kouketsu et al. 2011). The rate of observed ocean heat gain from 0–2000 m during 2006–2013, when Argo sampling of the ice-free ocean is near-global, is estimated at 0.5 ±0.1 W m^{-2} (Roemmich et al. 2015). Deep ocean warming, at least for 1992–2005, amounts to about 14% of that value. Because the global ocean is only sparsely sampled at decadal intervals by repeat hydrographic sections (Talley et al. 2016), presently direct estimates of deep ocean heat content can only be made retrospectively over decadal time scales.

Attempts to estimate deep ocean temperature changes as a residual (sea level changes from satellite data minus ocean mass changes from satellite data minus the steric expansion from 0–2000 m from Argo data) are stymied by large uncertainties and can result in an inferred small and statistically insignificant residual cooling from 2005–2013 (Llovel et al. 2014) or residual warming over a similar period (Dieng et al. 2015) that the authors note could also be arising from changes in marginal and shallow seas under-sampled by Argo. The variation in sign results mostly from differences in bias corrections for glacial isostatic adjustment, and the more general difficulty of inferring a relatively small value from the difference of larger ones. Hence, it is desirable to measure changes of deep ocean temperature (hence heat content and steric expansion) directly, the better to close global heat budgets and local sea level budgets.

Changes in temperature are also related to changes in circulation. In a simple budgetary calculation, the warming of abyssal waters of potential temperature < 0°C

105 originating around Antarctica implies a reduction in the volume of these waters at a rate
106 of around 8 Sv (1 Sv = 1×10^6 m^3 s^{-1}) from 1992–2005 (Purkey and Johnson 2012), with
107 an apparent slowdown of the northward flow of these waters across 35ºS in the Pacific
108 and western Atlantic at a rate of around 1 Sv $decade^{-1}$ in each of those basins from 1968–
109 2006 (Kouketsu et al. 2011). The Atlantic meridional overturning circulation also varies
110 on a variety of time scales, with southward flow of lower North Atlantic Deep Water
111 across 26ºN slowing by 7% per year from April 2004–October 2012 (Smeed et al. 2014).
112 These changes have obvious ramifications for the storage and cycling of heat, carbon,
113 and other climate-relevant parameters, as well as sea-surface temperatures (Cunningham
114 et al. 2013) and even decadal climate prediction (Msadek et al. 2011, Yeager et al. 2012,
115 Robson et al. 2012).
116 The renewed recognition of these dynamic, climate-relevant deep variations in
117 temperature, salinity, and circulation below 2000 m has led to a call for a "Deep Argo"
118 array (Johnson and Lyman 2014), to measure continuously the bottom half of the global
119 ocean volume below 2000 m, currently sampled only sparsely at decadal intervals by
120 repeat hydrography (Tally et al. 2016). Deep Argo floats require improvements in float
121 and sensor technology. While 2000-dbar floats use aluminum cylinders for pressure
122 cases, the 6000-dbar-capable Deep Argo floats use glass spheres because they better
123 withstand high pressures and more closely match the compressibility of seawater,
124 increasing energy efficiency. To detect the smaller signals in the deep ocean, CTDs used
125 for Deep Argo will also require more accurate (±3 dbar) pressure, temperature
126 (±0.001ºC) and salinity (±0.002 PSS-78) measurements with 6000-dbar capable sensors.

127 In addition to these hardware improvements, to design an effective Deep Argo array, it is
128 important to assess anticipated signals, noise levels, and scales of variability.
129 Here we use data mostly from a 1990s global survey of closely spaced hydrographic
130 sections (WOCE) and repeats of a key subset of those sections during the 2000s
131 (CLIVAR) and 2010s (GO-SHIP) along with data from Argo floats to inform the design
132 of a future Deep Argo array. We estimate temperature variance in the deep (> 2000 m)
133 and abyssal (> 4000 m) ocean using the hydrographic section data. We estimate de-
134 correlation time scales (following von Storch and Zwiers 1999) from quasi-Lagrangian
135 Argo float temperature time-series at 1800 m. A global mean deep horizontal de-
136 correlation length scale of 160 km has already been estimated in a similar manner using
137 temperature data from twenty-eight repeated hydrographic sections each spanning at least
138 2000 km (Purkey and Johnson 2010). Hence as long as Deep Argo floats are separated
139 by more than 160 km, each can be assumed to provide spatially independent information.
140 In section 2 we detail the data used and their processing. In section 3 we detail the
141 analyses performed, including assessments of de-correlation time scales and the detection
142 limits for global decadal trends and the estimated uncertainties of global integrals of
143 annual ocean heat content anomalies and for a relatively sparse (5º × 5º × 15-day target)
144 straw-plan Deep Argo array (Fig. 1). In section 4 we present the results of these
145 calculations, and we discuss the ramifications in section 5.
146
147 **2. Data and Processing**
148 To evaluate deep and abyssal temperature variance, we use 24,710 CTD stations from
149 467 full-depth hydrographic sections sampled from 1975–2010 (Fig. 2). The data were

150 downloaded from http://cchdo.ucsd.edu/ in 2010. The CTD station data used are high
151 vertical (1–2 dbar) resolution, and are generally accurate to ±1–2 mºC in temperature,
152 about ±0.002-0.003 PSS-78, and ±3 dbar in pressure, near the Deep Argo accuracy
153 targets. These hydrographic sections are typically occupied at nominal horizontal
154 resolution of 55 km between stations (55 km is the mode of station spacing in the sections
155 used here), closer over rapidly changing bathymetry (mid-ocean ridges and continental
156 slopes), but occasionally stations are further apart. The mean station spacing for the
157 sections we use (limiting our calculations to regions along the sections where station
158 spacing is < 100 km) is 44 km, with a standard deviation of 24 km.
159 Potential temperature profiles from each station are first lowpassed vertically using a
160 20-dbar half-width hanning filter and sub-sampled at 50 dbar intervals. Such filtering is
161 often used to remove small vertical scale features when studying the larger scales, and
162 vertical resolution of 50 dbar is more than sufficient for quantification of global patterns
163 of deep temperature variance. A minimum of three measurements with a mean distance
164 of 6-2/3 dbar are required within 20 dbar of each interpolated pressure level. The data at
165 each pressure level are then highpassed along each hydrographic section using a 500-km
166 loess filter, requiring at least 10 measurements within 500 km of each station location for
167 consideration. The resulting temperature variances at each pressure level are averaged in
168 5º long. × 5º lat. bins. Bins with < 30 measurements are discarded as potentially
169 unreliable indicators of regional variance.
170 A comparison of the original, 500-km loess low-passed, and high-passed temperature
171 data (Fig. 3) along one synoptic hydrographic section illustrates how the subtracting the
172 low-passed field (Fig. 3b), an approximation of the smooth long-term mean, from the

173 original field (Fig. 3a) that includes mesoscale eddy signatures, leaves only these
174 energetic smaller-scale eddy signatures (Fig. 3c). The particular section shown, a
175 meridional one extending from 60ºS to Iceland nominally along 25ºW (Fig. 2, red dots),
176 is located in the dynamic western basins of the South Atlantic Ocean and the more
177 quiescent eastern basins of the North Atlantic. This section has been occupied several
178 times. Here we display data (Fig. 3) from the 2005 occupation of the southern portion
179 (Johnson and Doney 2006), and the 2003 occupation of northern portion in 2003
180 (Johnson et al. 2005).

181 The eddy signatures observed (Fig. 3c) are generally vertically coherent in the deep
182 ocean, resulting in a banded structure that illustrates the ~160-km lateral de-correlation
183 length scale previously estimated from global repeated hydrographic sections (Purkey
184 and Johnson 2010). Eddies are strongest in regions of high vertical gradient (Fig. 3b),
185 such as the deep thermocline between the Antarctic Bottom Water and the North Atlantic
186 Deep Water in the Brazil Basin (from 35ºS to the equator at around 4000 dbar), as well as
187 in energetic regions such as the Antarctic Circumpolar Current and western boundary
188 current extension south of 40ºS, underneath the North Atlantic Current from 30ºN–40ºN,
189 and around the equator, where equatorial deep jets (Johnson and Zhang 2003) and the
190 flanking extra-equatorial jets (Gouriou et al. 1999) have strong density signatures. The
191 500-km smoother does a reasonable job of leaving only large-scale features. Even the
192 apparent undulations in the temperature field shallower than 3000 m from 20ºS to 5ºS are
193 long-term signatures of zonal currents that are reflected in water-property fields such as
194 salinity and dissolved oxygen (Talley and Johnson 1994). However, the large-scale filter
195 likely overestimates eddy variance around narrow boundary currents such as the cold

196 overflow evident on the continental rise from about 59ºN–62ºN, just south of Iceland (Fig.
197 3a), and the strong, sharp fronts of the Antarctic Circumpolar Current.
198 For calculating standard errors, we need estimates of de-correlation time scales in
199 addition to variance. For this purpose, we use Argo float data downloaded from an Argo
200 global data assembly center in January 2015, an initial total of 1,123,092 profiles from
201 10,090 floats. We consider only profile data with good quality control flags from float
202 cycles with position flags of either good, changed, or interpolated. We linearly interpolate
203 all data to 1800 dbar, discarding any profiles with vertical measurement spacing more
204 than 200 dbar around that pressure surface.
205
206 **3. Analysis**
207 We begin by assessing quasi-Langrangian de-correlation time scales for the 1800-
208 dbar temperature anomaly time series for each Argo float. To find the anomalies, we fit a
209 mean, trend, annual cycle, and semi-annual cycle to monthly gridded objective maps of
210 Argo temperature data from 2004–2014 (Roemmich and Gilson 2009) and subtract these
211 quantities from the float time series at each profile's time and location. These
212 calculations yield a set of time series of temperature anomalies at 1800 dbar for every
213 Argo float.
214 We consider only time series from floats where the mean time interval between
215 profiles is 12 days or less, the standard deviation of that time interval is one day or less,
216 less than 10% of the profiles for a given float have missing values, and the length of the
217 time series from that float is at least 10 times the estimated de-correlation time scale. This
218 screening retains data from 207,935 profiles from 1,575 floats, scattered around the globe.

219 We estimate the de-correlation time scale for each of these 1,575 temperature anomaly
220 time series as twice the maximum value of the integral of the normalized auto-correlation
221 sequence for the time series (von Storch and Zwiers 1999). We discuss details of the
222 results in the next section, but the resulting average value of 62 days for all the time
223 series is employed in the calculations described below.

224 We perform two different types of analyses, local and global, using the estimates of
225 deep temperature variance described above. Both analyses assume a relatively sparse
226 straw-plan Deep Argo array with 5º × 5º × 15-day sampling. With the present designs of
227 6000-dbar capable floats, 15-day sampling would provide a balance among the desire for
228 longevity (favoring at least a 5-year lifetime), concerns about sensor drift (favoring
229 lifetimes not much more than 5 years), and statistical independence of profiles (section 3).
230 Such an array, of about 1250 floats (excluding areas of the ocean shallower than 2000 m
231 or covered by sea-ice year-round), would resolve sub-basin scales and provide about
232 30,000 full-depth profiles per year. That is more data than from the WOCE, CLIVAR,
233 and GO-SHIP hydrographic sections (which took over three decades to collect) analyzed
234 here, and the deep Argo data would also be evenly distributed across the seasons (rather
235 than concentrated in the hemispheric summer as ship-based hydrographic section data
236 are) and more evenly distributed around the globe (rather than sampled densely along
237 quasi-synoptic sections with large gaps between them, as ship-based hydrographic data
238 usually are collected). For the local analyses we estimate statistical uncertainties for local
239 decadal temperature trends. For the global analyses we estimate statistical uncertainties
240 for global integrals of annual ocean heat content anomalies and annual thermosteric sea
241 level anomalies from 2000–6000 dbar.

242 We assume that at these space scales (5º × 5º), each sample is spatially statistically
243 independent. The 160-km global average lateral de-correlation length scale found using
244 repeat hydrographic section data (Purkey and Johnson 2010) certainly supports this
245 assumption, being considerably shorter than the hypothetically sparse sample array for
246 Deep Argo studied here. We also assume that the global mean de-correlation time scale
247 for the deep ocean is about 62 days, the value estimated from the average of Argo float
248 temperature anomaly time-series at 1800 dbar.
249 For both the local and global calculations we use the variance estimates to calculate
250 yearly uncertainties, assuming that every two months of data in each 5º × 5º bin are
251 independent when calculating standard errors of the mean at each location. We then
252 estimate the standard error for a decadal trend (from 10 sequential annual averages) using
253 a weighted least squares linear fit (e.g., Wunsch 1996). The standard error of this fit
254 depends only on the weights used (the inverse of the squared standard errors of the mean),
255 so calculating an actual trend or the residuals is not necessary.
256 For the local calculations, this exercise is carried out at each pressure level and each
257 grid point where 30 or more observations from hydrographic sections are available for
258 estimating the temperature variance.
259 For the global integrals, we linearly interpolate the variance estimates to unsampled
260 or undersampled bins on each horizontal level. However, we do not extrapolate poleward
261 of where we have samples in any ocean. Thus we scale integrated uncertainties at each
262 pressure level by the ratio of the total ocean volume at each pressure level (determined by
263 the bathymetry) to the sampled ocean volume (determined by bathymetry and the
264 requirement that bins contain 30 or more temperature estimates). For these global

265 integrals we assume that uncertainties are completely correlated in the vertical. Thus
266 during the vertical integrals, errors are summed. This assumption is consistent with the
267 vertically banded structure of eddy energy in the synoptic hydrographic sections (Fig. 3c).
268 However, based on the fact that the array density is much less than the average 160 km
269 de-correlation length scale, we also assume that uncertainties are completely uncorrelated
270 laterally, hence the vertically volume-integrated uncertainties are propagated as the
271 square root of the sum of the squares (i.e., added in quadrature) when integrating
272 horizontally (e.g., Taylor 1980). For the global heat content calculations we assume a
273 constant surface-referenced heat capacity of 3987 J kg^{-1} $ºC^{-1}$ and a constant in situ density
274 of 1043 kg m^{-3}. We estimate these constants from volume-weighted averages for the
275 global ocean deeper than 2000 m using a hydrographic climatology (Gouretski and
276 Kolterman 2004) and the 1980 equation of state (EOS-80). For the uncertainty of the
277 global thermosteric sea level integral we estimate the local thermal expansion coefficients
278 using the mean observed salinity and temperature values, along with the appropriate
279 pressure value and EOS-80.
280
281 **4. Results**
282 The quasi-Langrangian de-correlation time scales estimated for the 1800-dbar
283 temperature anomaly time series from Argo floats exhibit a distribution skewed toward
284 longer values (Fig. 4). While the mean time scale is 62 days, the median is only 54 days,
285 and the mode is around 40 days. Only 10% of the values are below 28 days, and only
286 10% exceed 107 days. In addition, there are noticeable spatial variations in the de-
287 correlation time scale (Fig. 5), with lower values in the tropics and along the western

boundary of the North Pacific, and higher values in the interior of the North Pacific and at higher latitudes, as might be expected given generally higher eddy energy levels at western boundaries and around the equatorial waveguide. There are slight hints of shorter time-scales at the western boundaries of other basins, but the most robust global pattern is shorter time scales within 15° latitude of the equator, and slightly longer time-scales at higher latitudes (Figs. 4 and 5). The 395 time-series with mean latitudes within 15° of the equator have a mean de-correlation time-scale of 47 days, a median of 41 days, and a mode around 30 days. The other 1,180 time-series at higher latitudes have a mean de-correlation time scale of 67 days, a median of 60 days, and a mode around 40 days.

To be conservative, and for simplicity, we assume 6 independent samples per year for Deep Argo floats, based upon the global mean time scale of 62 days. However, since standard errors scale as the inverse of the square root of the number of independent samples, the results are not overly sensitive to this assumption. Even for a 28-day time scale estimated uncertainties would only be reduced by about 33%, whereas for a 107-day time scale they would only be inflated by about 31%.

We estimate uncertainties of decadal deep ocean temperature trends for the straw-plan Deep Argo array using the local variances and global mean de-correlation space and time scale estimates detailed above. The uncertainties vary by an order of magnitude both vertically (Fig. 6) and laterally (Fig. 7). Meridional-vertical sections of zonal averages of uncertainties in decadal temperature trends for the three major oceans (Fig. 6) show a general pattern of decreasing uncertainties with increasing pressure, likely owing to the overall reduction in vertical temperature gradient with increasing depth. There is a maximum in deep uncertainties in the latitude range of the relatively vigorous Antarctic

311 Circumpolar Current and western boundary current extensions (60ºS–40ºS), with a
312 meridional maximum of zonally and depth-averaged values below 2000 dbar of 26 mºC
313 decade^{-1} at 50ºS. There are also indications of an equatorial maximum in the Atlantic and
314 Pacific Oceans, consistent with the presence of vigorous time-dependent equatorial
315 features such as the equatorial deep jets (e.g., Youngs and Johnson 2015). The northern
316 North Atlantic, with its deep thermocline and relatively strong deep vertical temperature
317 gradients, also exhibits relatively high values from 30–70ºN, with lower values in the
318 deep Greenland-Iceland-Norwegian Seas. The abyssal North Pacific Ocean has the
319 lowest noise values, in places < 1 mºC decade^{-1}.
320 Maps of uncertainties for decadal temperature trends at 3000 and 4000 dbar (Fig. 7)
321 reveal patterns similar to the zonal averages, but providing detail as to zonal variations.
322 The eastern portions of the oceans are generally more quiescent that the western portions,
323 as might be expected given the existence of vigorous western boundary currents. The
324 band of high uncertainties associated with the Antarctic Circumpolar Current and the
325 Northern North Atlantic, two locations where currents are very deep reaching, are also
326 apparent.
327 Global integrals of heat content uncertainties for pressures of 2000–6000 dbar have a
328 yearly uncertainty of 1 ZJ (1 ZJ = 10^{21} J) standard error of the mean, resulting in a formal
329 decadal trend standard error of 3 TW (1 TW = 10^{12} W). For the uncertainty of the
330 thermosteric contribution to globally averaged sea level over that same pressure range,
331 the uncertainty is 0.1 mm annually, resulting in a formal decadal trend standard error of
332 ±0.1 mm decade^{-1}.
333

5. Discussion

Here we estimate quasi-Lagrangian de-correlation time scales from Argo float deep (1800 dbar) temperature anomaly time series and temperature variance using 500-km high-passed WOCE and GO-SHIP hydrographic section data averaged in 5º x 5º bins to assess noise levels. The spatial pattern of deep de-correlation time scales (Fig. 5) is perhaps not surprising, with shorter values near the eddy-richer western boundaries and around the energetic equatorial wave-guide, and longer values in the more quiescent eastern sides of basins at higher latitudes.

The 62-day global mean value of the de-correlation time scales means that for a profiling interval of 15 days, on average about every fourth profile would be independent, resolving some of the temporal variability. Around western boundaries and the equator, each deep Argo profile might be closer to being a statistically independent sample than on the eastern sides of basins at higher latitudes. One could attempt to use a map of the de-correlation time scales to refine regional uncertainty estimates, but since standard errors scale as the inverse square root of the number of independent samples, the results are not especially sensitive to the use of a mean value instead of a regionally varying one.

While the vertically banded nature of high-passed temperatures in the synoptic hydrographic section data (e.g., Fig. 3c) suggest the de-correlation time scales at 1800 dbar may be typical of Deep Argo floats at greater depths, it is also possible that different choices of parking depths for the Deep Argo floats, or perhaps the time spent profiling in regions of varying shear, may change the de-correlation time scales from deep Argo floats compared to those from Argo floats at 1800 m, another argument for simply using the global mean de-correlation time scale.

357 One could also attempt to estimate de-correlation time scales from deep moored
358 temperature time-series, but a few confounding factors would make those less relevant
359 for the study at hand than those estimated from the Argo float time-series. First, the
360 decadal time-series of Argo data allow removal of estimates of the seasonal cycle from
361 the float time-series, something that would not be possible from most moored time-series,
362 which are not often longer than a year to two in duration. That inability to remove the
363 seasonal cycle would likely bias the de-correlation time scales from the moored time-
364 series toward long values. Second, deep moored temperature records typically do not
365 extend over much more than a year to two, and those short records could hinder robust
366 estimates of de-correlation time scales. Third, vertical mooring motion can introduce
367 spurious variance into temperature records (Meinen 2008), an artifact not present in float
368 profiles. Finally, floats sample temperature close to instantaneously, whereas some
369 current meter data are low-passed to filter out higher-frequency variability, so the float
370 data contain variance from these phenomena that would be reduced in low-passed current
371 meter data.

372 Array design depends on the questions to be answered. Here we cast our findings
373 simply, in terms of local and global decadal trends detectable above one standard error of
374 the mean for a 5º × 5º × 15-day Deep Argo array (Fig. 1) using estimated 160-km spatial
375 and two-monthly temporal de-correlation scales (the latter based on the global mean
376 value of 62 days estimated using temperature anomaly time series at 1800 dbar from
377 Argo floats). Such an array would be capable of resolving, on average, local trends of <
378 1 mºC decade^{-1} in the abyssal Pacific and at worst around 26 mºC decade^{-1} zonally and
379 depth averaged below 2000 dbar along 50ºS, in the energetic deep Southern Ocean.

380 Decadal trends from 1992–2005 have been estimated at 5 mºC decade^{-1} in the global
381 abyssal ocean, and 30 mºC decade^{-1} in the deep Southern Ocean using repeat
382 hydrographic data (Purkey and Johnson 2010). That analysis required large-scale (basin,
383 ocean, or global) averages to find statistically significant results. In contrast, the straw-
384 plan deep Argo array would be capable of detecting anticipated decadal trends *locally* at
385 5º x 5º resolution on decadal time scales.
386 The trend in deep (> 2000 dbar) global ocean heat gain for from 1992–2005 was
387 assessed at +35 (±17) TW (one standard error uncertainty) using repeat hydrographic data
388 (Purkey and Johnson 2010). The deep (> 2000 dbar) global ocean trend in heat gain for
389 2005–2013 is estimated at -40 (±220) TW (one standard error uncertainty) from a
390 residual of 0–2000-m Argo steric expansion, ocean mass change estimates from GRACE
391 satellite gravimetry, and ocean sea level change estimates from satellite altimetry (Llovel
392 et al. 2014). The straw-plan Argo array here, fully implemented for a decade, could
393 provide annual values to within a yearly one standard error uncertainty of 1 ZJ and hence
394 a deep (>2000 dbar) global ocean heat trend to within ±3 TW, a large improvement over
395 the direct estimate from repeat hydrography and a huge improvement over the residual
396 calculation.
397 Similarly, the contribution of deep (> 2000 dbar) ocean thermal expansion on the
398 global sea level rise could be determined to a standard error of 0.1 mm annually, with a
399 trend standard error of ±0.1 mm decade^{-1}. These numbers compare with a repeat
400 hydrographic trend standard error of ±0.5 mm decade^{-1} (Purkey and Johnson 2010) and a
401 trend standard error of ±7 mm decade^{-1} for the satellite-Argo residual calculation (Llovel
402 et al. 2014). These full-depth steric expansion fields, together with sea-surface height

403 fields from satellite altimetry, would allow a very precise assessment of spatio-temporal
404 variations in sea level, including those expected from changes in the gravity field with
405 melting glaciers and ice sheets (Bamber and Riva 2010).
406 There are certainly other benefits of a deep Argo array that are not assessed here. As
407 mentioned in the introduction, there are considerable changes observed in the deep
408 meridional overturning circulation of both the North Atlantic Deep Water and the
409 Antarctic Bottom Water in recent decades, but these are sampled only decadally by repeat
410 hydrographic sections (Purkey and Johnson 2012) or locally by moored arrays (Smeed et
411 al. 2014). Deep Argo would measure these changes globally and continuously. In
412 addition, there are large salinity changes in components of North Atlantic Deep Water
413 (Yashayaev 2007) as well as Antarctic Bottom Water in the Pacific (Swift and Orsi 2012),
414 Indian (Aoki et al. 2005), and perhaps even Atlantic (Jullion et al. 2013) oceans that Deep
415 Argo would also measure globally and continuously.
416 Of course, Deep Argo data would complement, and not supplant, repeat hydrographic
417 section data. Repeat hydrographic section data provide the highly accurate and traceable
418 salinity data required to check and adjust Argo (and Deep Argo) conductivity sensor data
419 (Wong et al. 2003). Furthermore, repeat hydrographic sections, when quasi-synoptic,
420 full-depth, and coast-to-coast, allow for well-constrained transport estimates including
421 boundary currents (Ganachaud 2003) that Argo and Deep Argo resolve less well. Repeat
422 hydrographic sections also collect data on other water properties that allow for direct
423 estimates of ocean carbon uptake (Sabine and Tanhua 2010), ocean acidification, (Byrne
424 et al. 2010), long-term changes in dissolved oxygen concentration (Stramma et al. 2008),
425 as well as estimates of changes in ocean circulation and ventilation from transient tracers

426 (Fine 2011). Deep Argo would provide well-resolved temperature, salinity, and perhaps
427 dissolved oxygen fields, allowing improved inventory estimates for ocean water
428 properties when combined with the repeat hydrographic section data.
429
430 *Acknowledgments:*
431 We thank everyone who helped to collect, calibrate, process, and archive the WOCE,
432 CLIVAR, and GO-SHIP hydrographic section data. Argo data are collected and made
433 freely available by the International Argo Program, which is part of the Global Ocean
434 Observing System, and the national programs that contribute to it
435 (http://www.argo.ucsd.edu, http://argo.jcommops.org). GCJ and JML are supported
436 by the NOAA Climate Program Office and NOAA Research. SGP is supported through
437 an LDEO Postdoctoral Fellowship.
438
439 REFERENCES
440 Aoki, S., S. R. Rintoul, S. Ushio, S. Watanabe, and N. L. Bindoff, 2005: Freshening of
441 the Adelie Land Bottom Water near 140ºE. *Geophys. Res. Lett.*, **32**, L23601,
442 doi:10.1029/2005GL024246.
443 Bamber, J., and R. Riva, 2010: The sea level fingerprint of recent ice mass fluxes. *The*
444 *Cryosphere*, **4,** 621–627, doi:10.5194/tc-4-621-2010.
445 Byrne, R. H., S. Mecking, R. A. Feely, and X. Liu, 2010: Direct observations of basin-
446 wide acidification of the North Pacific Ocean. *Geophys. Res. Lett.*, **37**, L02601,
447 doi:10.1029/2009GL040999.

448 Cunningham, S. A., and Coauthors, 2013: Atlantic Meridional Overturning Circulation
449 slowdown cooled the subtropical ocean. *Geophys. Res. Lett.*, **40,** 6202–6207,
450 doi:10.1002/2013GL058464.
451 Dieng, H. B., H. Palanisamy, A. Cazenave, B. Meyssignac, and K. von Schuckmann,
452 2015: The Sea Level Budget Since 2003: Inference on the Deep Ocean Heat Content.
453 *Surv. Geophys.*, **36,** 209–229, doi:10.1007/s10712-015-9314-6.
454 Fine, R. A., 2011: Observations of CFCs and SF6 as Ocean Tracers. *Annu. Rev. Mar. Sci.,*
455 **3,** 173–195, doi:10.1146/annurev.marine.010908.163933.
456 Ganachaud, A., 2003: Large-scale mass transports, water mass formation, and
457 diffusivities estimated from World Ocean Circulation Experiment (WOCE)
458 hydrographic data. *J. Geophys. Res.*, **108,** 3213, doi:10.1029/2002JC001565.
459 Gordon, A. L., 1982: Weddell Deep Water variability. *J. Mar. Res.*, **40,** 199–217.
460 Gouretski, V. V., and K.P. Koltermann, 2004: *WOCE Global Hydrographic Climatology.*
461 35/2004, Berichte des Bundesamtes fur Seeschifffahrt und Hydrographie, 52 pp.
462 Gouriou, Y., B. Bourles, H. Mercier, and R. Chuchla, 1999: Deep jets in the equatorial
463 Atlantic Ocean. *J. Geophys. Res.*, **104,** 21217–21226, doi:10.1029/1999JC900057.
464 Johnson, G. C., 2008: Quantifying Antarctic Bottom Water and North Atlantic Deep
465 Water volumes. *J. Geophys. Res.*, **113,** C05027, doi:10.1029/2007JC004477.
466 Johnson, G. C., and D. X. Zhang, 2003: Structure of the Atlantic Ocean equatorial deep
467 jets. *J. Phys. Oceanogr.*, **33,** 600–609, doi:10.1175/1520-
468 0485(2003)033<0600:SOTAOE>2.0.CO;2.
469 Johnson, G. C., and S. C. Doney, 2006: Recent western south Atlantic bottom water
470 warming. *Geophys. Res. Lett.*, **33**, L21604, doi:10.1029/2006GL028294.

471 Johnson, G. C., and J. M. Lyman, 2014: OCEANOGRAPHY Where's the heat? *Nature*
472 *Climate Change*, **4,** 956–957, doi:10.1038/nclimate2409.
473 Johnson, G. C., J. L. Bullister, and N. Gruber, 2005: Labrador Sea Water property
474 variations in the northeastern Atlantic Ocean. *Geophys. Res. Lett.*, **32**, L07602,
475 doi:10.1029/2005GL022404.
476 Jullion, L., A. C. N. Garabato, M. P. Meredith, P. R. Holland, P. Courtois, and B. A. King,
477 2013: Decadal Freshening of the Antarctic Bottom Water Exported from the Weddell
478 Sea. *J. Climate*, **26,** 8111–8125, doi:10.1175/JCLI-D-12-00765.1.
479 Klatt, O., O. Boebel, and E. Fahrbach, 2007: A profiling float's sense of ice. *J. Atmos.*
480 *Oceanic Tech.*, **24,** 1301–1308, doi:10.1175/JCLI-D-12-00765.1.
481 Kouketsu, S., and Coauthors, 2011: Deep ocean heat content changes estimated from
482 observation and reanalysis product and their influence on sea level change. *J.*
483 *Geophys. Res.*, **116,** C03012, doi:10.1029/2010JC006464.
484 Llovel, W., J. K. Willis, F. W. Landerer, and I. Fukumori, 2014: Deep-ocean contribution
485 to sea level and energy budget not detectable over the past decade. *Nature Climate*
486 *Change*, **4,** 1031–1035, doi:10.1038/nclimate2387.
487 Lumpkin, R., and K. Speer, 2007: Global ocean meridional overturning. *J. Phys.*
488 *Oceanogr.*, **37,** 2550–2562, doi:10.1175/JPO3130.1.
489 Mauritzen, C., A. Melsom, and R. T. Sutton, 2012: Importance of density-compensated
490 temperature change for deep North Atlantic Ocean heat uptake. *Nature Geosci.*, **5,**
491 905–910, doi:10.1038/ngeo1639.
492 Meinen, C. S., 2008: Accuracy in Mooring Motion Temperature Corrections. *J. Atmos.*
493 *Oceanic Techn.*, **25,** 2293–2303, doi:10.1175/2008JTECHO555.1.

494 Msadek, R., C. Frankignoul, and L. Z. X. Li, 2011: Mechanisms of the atmospheric
495 response to North Atlantic multidecadal variability: a model study. *Climate Dynam.*,
496 **36,** 1255–1276, doi:10.1007/s00382-010-0958-0.
497 Orsi, A. H., G. C. Johnson, and J. L. Bullister, 1999: Circulation, mixing, and production
498 of Antarctic Bottom Water. *Prog. Oceanogr.*, **43,** 55–109, doi:10.1016/S0079-
499 6611(99)00004-X.
500 Purkey, S. G., and G. C. Johnson, 2010: Warming of Global Abyssal and Deep Southern
501 Ocean Waters between the 1990s and 2000s: Contributions to Global Heat and Sea
502 Level Rise Budgets. *J. Climate*, **23,** 6336–6351, doi:10.1175/2010JCLI3682.1.
503 ——, 2012: Global Contraction of Antarctic Bottom Water between the 1980s and 2000s.
504 *J. Climate*, **25,** 5830–5844, doi:10.1175/JCLI-D-11-00612.1.
505 Rhein, M., and Coauthors, 2013: Observations: Ocean. *Climate Change 2013: The*
506 *Physical Science Basis. Contribution of Working Group I to the Fifth Assessment*
507 *Report of the Intergovernmental Panel on Climate Change*, T. F. Stocker, and
508 Coauthors, Eds., Cambridge University Press, 255–315,
509 doi:10.1017/CBO9781107415324.010.
510 Robson, J. I., R. T. Sutton, and D. M. Smith, 2012: Initialized decadal predictions of the
511 rapid warming of the North Atlantic Ocean in the mid 1990s. *Geophys. Res. Lett.*, **39,**
512 L19713, doi:10.1029/2012GL053370.
513 Roemmich, D., and J. Gilson, 2009: The 2004-2008 mean and annual cycle of
514 temperature, salinity, and steric height in the global ocean from the Argo Program.
515 *Prog. Oceanogr.*, **82,** 81–100, doi:10.1016/j.pocean.2009.03.004

516 Roemmich, D., J. Church, J. Gilson, D. Monselesan, P. Sutton, and S. Wijffels, 2015:
517 Unabated planetary warming and its ocean structure since 2006. *Nature Climate*
518 *Change*, **5,** 240–245., doi:10.1038/nclimate2513.
519 Roemmich, D., and Coauthors, 2009: The Argo Program Observing the Global Ocean
520 with Profiling Floats. *Oceanogr.*, **22(2),** 34–43, doi:10.5670/oceanog.2009.36.
521 Sabine, C. L., and T. Tanhua, 2010: Estimation of Anthropogenic CO_2 Inventories in the
522 Ocean. *Annu. Rev. Mar. Sci.*, **2,** 175–198, doi:10.1146/annurev-marine-120308-
523 080947.
524 Smeed, D. A., and Coauthors, 2014: Observed decline of the Atlantic meridional
525 overturning circulation 2004-2012. *Ocean Sci.*, **10,** 29–38, doi:10.5194/os-10-29-
526 2014:
527 Smith, T. M., R. W. Reynolds, T. C. Peterson, and J. Lawrimore, 2008: Improvements to
528 NOAA's historical merged land-ocean surface temperature analysis (1880–2006). *J.*
529 *Climate*, **21,** 2283–2296, doi:10.1175/2007JCLI2100.1.
530 Somavilla, R., U. Schauer, and G. Budeus, 2013: Increasing amount of Arctic Ocean
531 deep waters in the Greenland Sea. *Geophys. Res. Lett.*, **40,** 4361–4366, doi:
532 10.1002/grl.50775.
533 Stramma, L., G. C. Johnson, J. Sprintall, and V. Mohrholz, 2008: Expanding oxygen-
534 minimum zones in the tropical oceans. *Science*, **320,** 655–658,
535 doi:10.1126/science.1153847.
536 Swift, J. H., and A. H. Orsi, 2012: Sixty-Four Days of Hydrography and Storms: RVIB
537 Nathaniel B. Palmer's 2011 S04P Cruise. *Oceanogr.*, **25(3),** 54–55,
538 doi:10.5670/oceanog.2012.74.

539 Talley, L. D., and co-authors, 2016: Changes in ocean heat, carbon content, and
540 ventilation: A review of the first decade of GO-SHIP Global Repeat Hydrography.
541 *Ann. Rev. Mar. Sci.*, **8**, in press, doi:10.1146/annurev-marine-052915-100829.
542 Talley, L. D., and G. C. Johnson, 1994: Deep, zonal subequatorial currents. *Science*, **263,**
543 1125–1128, doi:10.1126/science.263.5150.1125.
544 Taylor, J. R., 1980: *An Introduction to Error Analysis: The Study of Uncertainties in*
545 *Physical Measurements*, Univ. Science Books, Mill Valley, California, pp. 69–72.
546 Toole, J. M., R. A. Krishfield, M. L. Timmermans, and A. Proshutinsky, 2011: The ice-
547 tethered profiler: Argo of the arctic. *Oceanogr.*, **24(3),** 126–135,
548 doi:10.5670/oceanog.2011.64.
549 von Storch, H., and F. W. Zwiers, 1999: *Statistical Analysis in Climate Research.*
550 Cambridge University Press, Cambridge, U. K., 484 pp.
551 Wong, A. P. S., G. C. Johnson, and W. B. Owens, 2003: Delayed-mode calibration of
552 autonomous CTD profiling float salinity data by theta-S climatology. *J. Atmos.*
553 *Oceanic Techn.*, **20,** 308–318, doi:10.1175/1520-
554 0426(2003)020<0308:DMCOAC>2.0.CO;2.
555 Wunsch, C., 1996: *The Ocean Circulation Inverse Problem*, Cambridge Univ. Press,
556 Cambridge, U. K., 442 pp.
557 Yashayaev, I., 2007: Hydrographic changes in the Labrador Sea, 1960-2005. *Prog.*
558 *Oceanogr.*, **73,** 242–276, doi:10.1016/j.pocean.2007.04.015.
559 Yeager, S., A. Karspeck, G. Danabasoglu, J. Tribbia, and H. Y. Teng, 2012: A Decadal
560 Prediction Case Study: Late Twentieth-Century North Atlantic Ocean Heat Content. *J.*
561 *Climate*, **25,** 5173–5189, doi:10.1175/JCLI-D-11-00595.1.

562 Youngs, M. K., and G. C. Johnson, 2015: Basin-wavelength Equatorial Deep Jet Signals
563 across Three Oceans. *J. Phys. Oceanogr.*, **45**, 2134–2148, doi:10.1175/JPO-D-14-
564 0181.1.

565

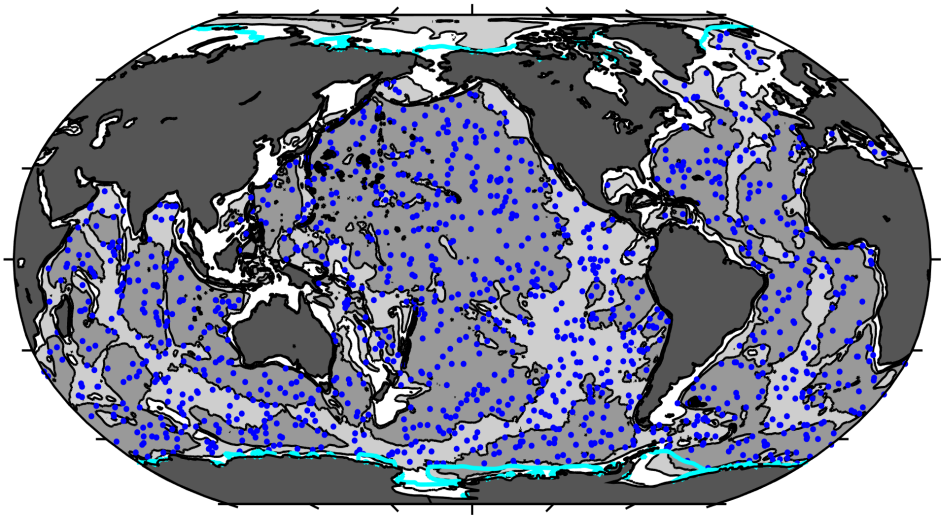

566

567 FIG. 1. Straw-plan of a nominally 5º x 5º distribution of 1228 Deep Argo floats (blue
568 dots) randomly populating the global ocean excluding areas shallower than 2000 m
569 (white areas), and areas with mean 1981–2010 ice concentrations > 75% (poleward of
570 thick cyan contours). Lightest gray areas indicate bottom depths between 2000 and 4000
571 m, darker gray areas indicate bottom depths exceeding 4000 m, and darkest gray areas
572 indicate land.

573

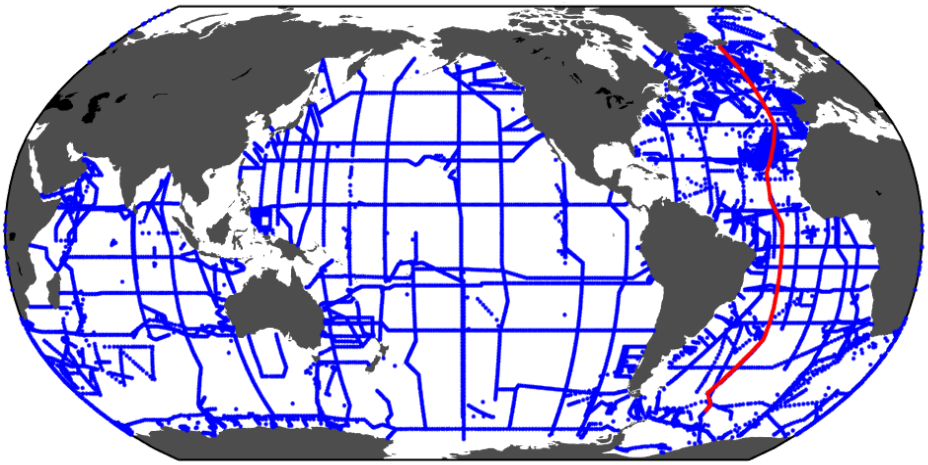

574

575 FIG. 2. Map of station positions for the CTD profiles used in this study (blue dots). The

576 WOCE A16 hydrographic section is highlighted by color (red dots).

577

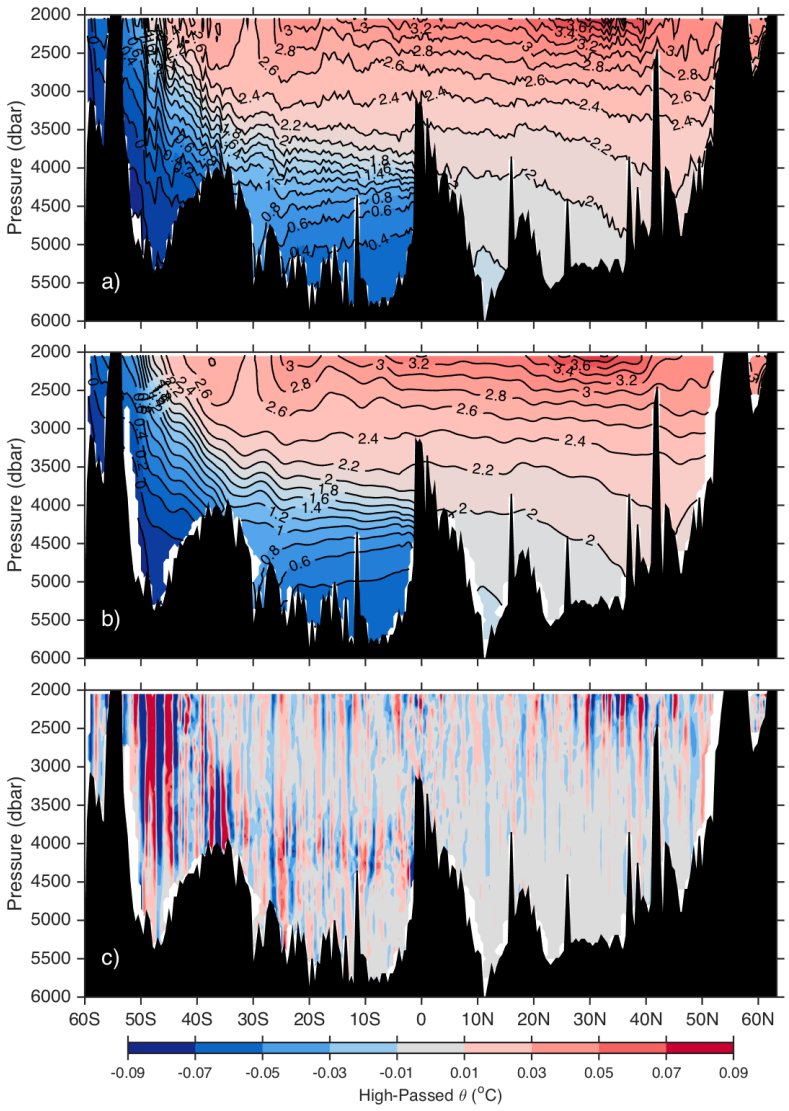

578

579 FIG. 3. Pressure-latitude sections of potential temperature along WOCE hydrographic

580 section A16, nominally along 25ºW in the Atlantic (Fig. 2, red dots), using the 2003 data

581 in the North Atlantic (Johnson et al. 2005), and the 2005 data in the South Atlantic

582 (Johnson and Doney 2006). (a) The unsmoothed data, contoured at 0.2ºC intervals. (b)

583 The data horizontally low-pass filtered using a 500-km loess filtered data contoured at the

584 same intervals. (c) The data horizontally high-pass filtered by subtracting (b) from (a),

585 contoured at 0.02ºC intervals (see colorbar).

586

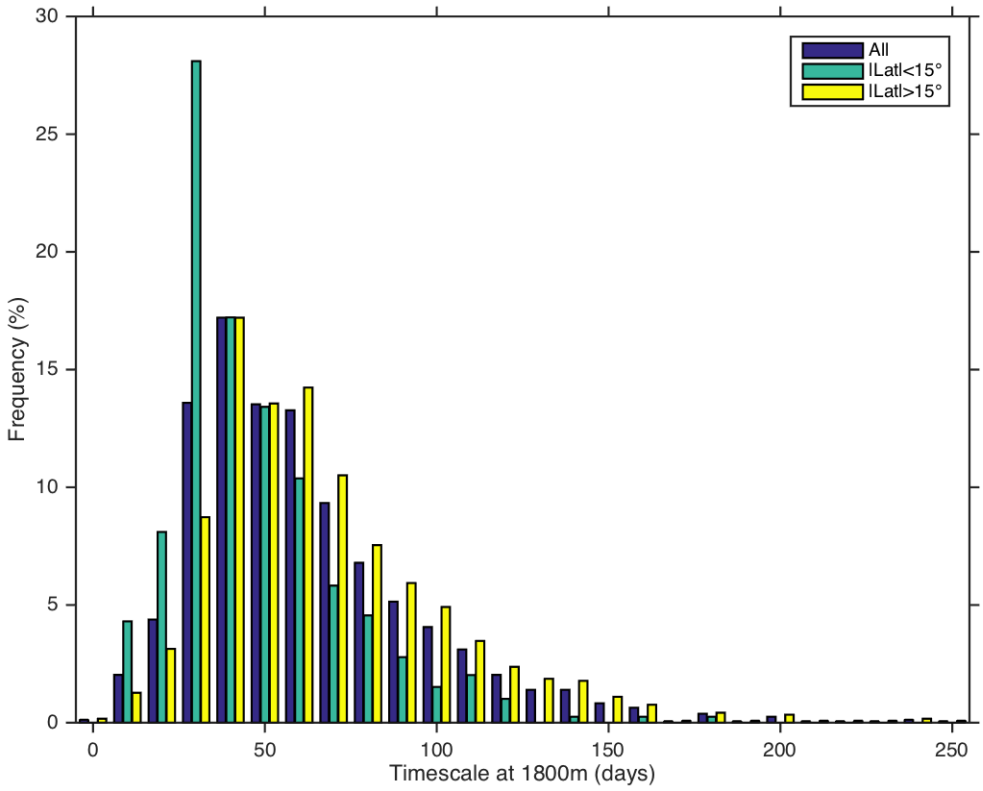

587

588 FIG. 4. Histograms of de-correlation time scales in 10-day bins estimated from
589 temperature anomaly time series at 1800 dbar from a screened subset of 1,575 Argo
590 floats around the globe (blue bars, left of bin centers; Fig. 5), the 395 floats with mean
591 latitudes within 15° of the equator (green bars, bin-centered), and the remaining 1180
592 with mean latitudes outside of that near-equatorial band (yellow bars, right of bin centers).

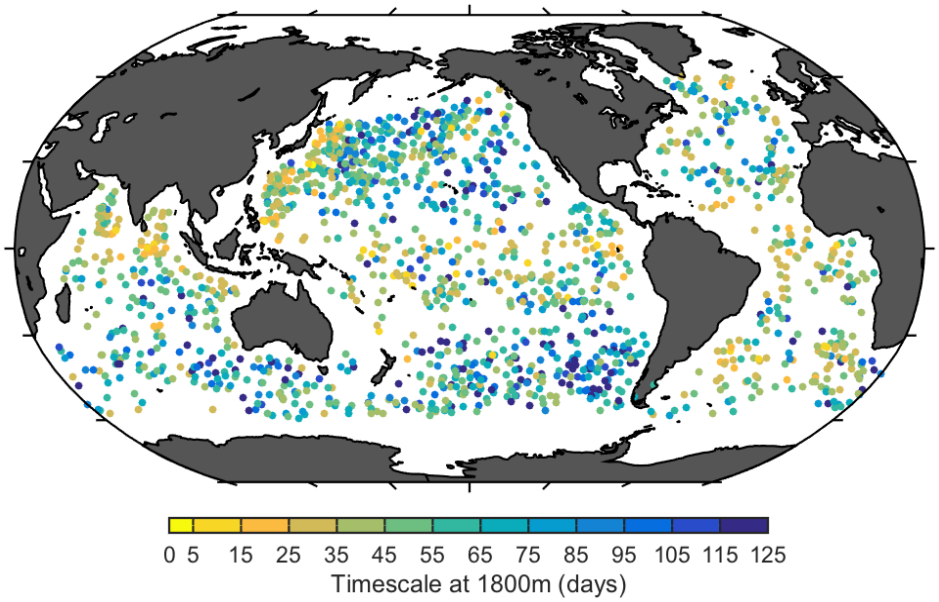

FIG. 5. De-correlation time scales (colorbar) estimated from temperature anomaly time series at 1800 dbar from a screened subset of 1,575 Argo floats, plotted at mean locations of the profiles comprising the time-series for each Argo float.

598

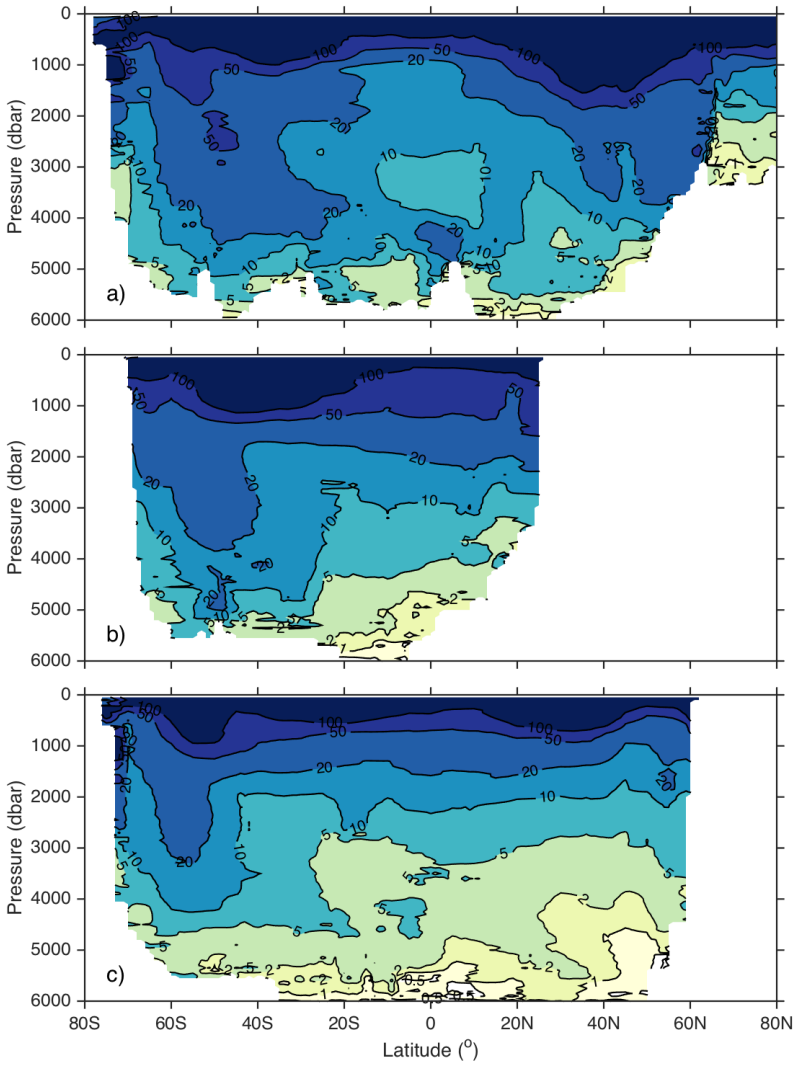

599

600 FIG. 6. Meridional-vertical sections (latitude vs. pressure) of zonal averages of estimated

601 decadal temperature trend standard errors in m°C decade^{-1} for the (a) Atlantic, (b)

602 Indian, and (c) Pacific oceans. Contours (labeled) are at approximately logarithmic

603 intervals.

604

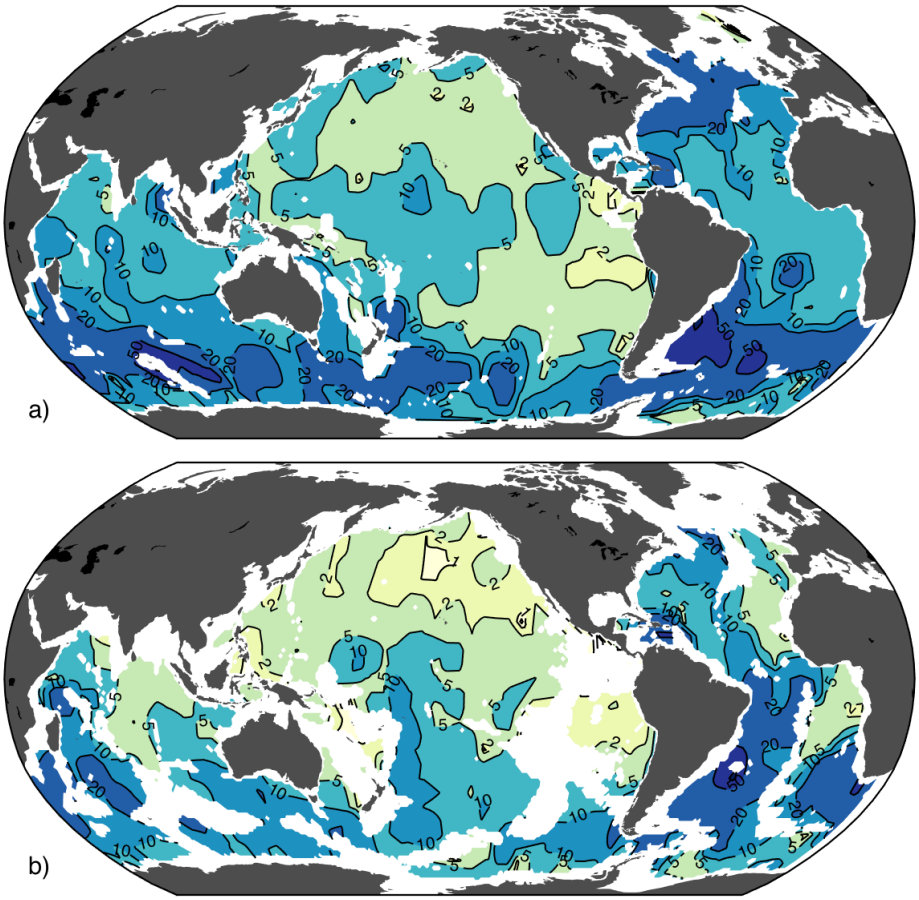

605

606 FIG. 7. Maps of estimated temperature trend standard errors in mºC decade^{-1} at (a) 3000

607 dbar and (b) 4000 dbar. Bins with fewer than 30 measurements are not included, and

608 values in unsampled or undersampled bins are linearly interpolated from surrounding

609 well-sampled bins. Contours (labeled) are at approximately logarithmic intervals.